Autonomic closure for turbulence simulations

Ryan N. King, Peter E. Hamlington, and Werner J. A. Dahm

Phys. Rev. E **93**, 031301 — Published 14 March 2016

DOI: 10.1103/PhysRevE.93.031301

Autonomic Closure for Turbulence Simulations

Ryan N. King[1,2], Peter E. Hamlington[1],* and Werner J.A. Dahm[3]

[1]*Department of Mechanical Engineering, University of Colorado, Boulder, CO 80309*

[2]*National Renewable Energy Laboratory, Golden, Colorado 80401 and*

[3]*School for Engineering of Matter, Transport, & Energy, Arizona State University, Tempe, AZ 85287*

Abstract

A new approach to turbulence closure is presented that eliminates the need to specify a predefined turbulence model and instead provides for fully-adaptive, self-optimizing, autonomic closures. The closure is autonomic in the sense that the simulation itself determines the optimal local, instantaneous relation between any unclosed term and resolved quantities through the solution of a nonlinear, nonparametric system identification problem. This nonparametric approach allows the autonomic closure to freely adapt to varying nonlinear, nonlocal, nonequilibrium, and other turbulence characteristics in the flow. Even a simple implementation of the autonomic closure for large eddy simulations provides remarkably more accurate results in *a priori* tests than do dynamic versions of traditional prescribed closures.

* Corresponding author: peh@colorado.edu

Introduction. Turbulence typically involves very wide ranges of length and time scales, which place an enormous computational burden on direct solutions of transport equations for momentum, energy, and scalars in turbulent flows. Coarse-graining [e.g., large eddy simulation (LES)] reduces this burden by solving equations for only intermediate and large scales, but nonlinearity in the original equations then introduces unclosed terms that must be modeled to achieve closure. For instance, with tildes denoting coarse-grained quantities, the incompressible momentum equation after low-pass filtering at scale $\widetilde{\Delta}$ is

$$\frac{\partial}{\partial t}\widetilde{u}_i + \widetilde{u}_j\frac{\partial}{\partial x_j}\widetilde{u}_i = -\frac{\partial}{\partial x_i}\widetilde{p} + \nu\frac{\partial^2}{\partial x_j^2}\widetilde{u}_i - \frac{\partial}{\partial x_j}\tau_{ij}\,, \tag{1}$$

where $\widetilde{u}_i(\mathbf{x},t)$ and $\widetilde{p}(\mathbf{x},t)$ are the "resolved" velocity and pressure, with the density absorbed in $\widetilde{p}$, and where $\tau_{ij} \equiv \widetilde{u_i u_j} - \widetilde{u}_i\widetilde{u}_j$ is the unclosed stress that accounts for local, instantaneous momentum exchange between resolved and unresolved scales. Coarse-graining of other transport equations introduces similar unclosed terms.

A central challenge in turbulence simulations is to achieve closure of coarse-grained equations by relating unclosed terms such as τ_{ij} to resolved quantities via turbulence models. Many such models have been proposed, particularly for use in LES, with the most common [1–4] prescribing τ_{ij} relations that depend only on the resolved strain rate tensor, as reviewed in [5]. However since coarse graining was introduced, more than 50 years of research has failed to provide universal models for τ_{ij} or other unclosed terms that reliably account for nonlinear, nonlocal, nonequilibrium, and other turbulence effects [6–8] with fidelity approaching that of direct simulation in the resolved scales at all local flow conditions.

Autonomic Closure Approach. Here we take a completely different approach to turbulence closure that circumvents the need to prescribe a fixed relation between unclosed terms and resolved variables. Rather than specifying a prescribed model for the unclosed stress τ_{ij} or other unclosed terms, we instead use a fully general nonparametric relation $\mathcal{F}$ that represents the true unclosed quantity in terms of all resolved variables at all points and all prior times. For example, to model τ_{ij} in incompressible turbulence this fully general nonparametric relation for the stress can be expressed as

$$\tau_{ij}^{\mathcal{F}}(\mathbf{x},t) \equiv \mathcal{F}_{ij}\left[\widetilde{\mathbf{u}}(\mathbf{x}+\mathbf{x}',t-t'),\, \widetilde{p}(\mathbf{x}+\mathbf{x}',t-t')\,\forall\,\mathbf{x}',t' \geq 0\right]\,, \tag{2}$$

where $(\mathbf{x}',t')$ is a stencil with center point $(\mathbf{x},t)$ on which the resolved variables in $\mathcal{F}_{ij}$ are defined and $\tau_{ij}^{\mathcal{F}}$ represents the true stress τ_{ij}. Due to its generality, $\mathcal{F}_{ij}$ will typically

have a very large number of degrees of freedom, and is thereby free to adapt to the local, instantaneous turbulence state in the flow.

The particular form of the general relation $\mathcal{F}_{ij}$ is determined at each point and time using system identification based on test filtering. Resolved variables are filtered at a test scale $\widehat{\Delta} > \widetilde{\Delta}$ to yield test-filtered resolved variables, such as $\widehat{\widetilde{\mathbf{u}}}(\mathbf{x},t)$ and $\widehat{\widetilde{p}}(\mathbf{x},t)$, which are then used to obtain a test field for the unclosed quantity; e.g., for $\tau_{ij} \equiv \widetilde{u_i u_j} - \widetilde{u}_i \widetilde{u}_j$ the test field is $T_{ij} \equiv \widehat{\widetilde{u}_i \widetilde{u}_j} - \widehat{\widetilde{u}}_i \widehat{\widetilde{u}}_j$. The same nonparametric relation $\mathcal{F}_{ij}$ introduced in Eq. (2) is used to relate the known test field to known test-filtered variables. Thus, for instance, analogous to Eq. (2)

$$T_{ij}^{\mathcal{F}}(\mathbf{x},t) \equiv \mathcal{F}_{ij}\left[\widehat{\widetilde{\mathbf{u}}}(\mathbf{x}+\mathbf{x}',t-t'), \widehat{\widetilde{p}}(\mathbf{x}+\mathbf{x}',t-t') \,\forall\, \mathbf{x}', t' \geq 0\right]. \tag{3}$$

Values for the degrees of freedom in $\mathcal{F}_{ij}$ are determined by optimizing the local, instantaneous agreement of $T_{ij}^{\mathcal{F}}$ with T_{ij} via minimization of a suitably defined objective function

$$\mathcal{J}_{ij}(\mathbf{x},t) = E\left[T_{ij}(\mathbf{x},t), T_{ij}^{\mathcal{F}}(\mathbf{x},t)\right] \tag{4}$$

that measures the error in representing $T_{ij}(\mathbf{x},t)$ with $T_{ij}^{\mathcal{F}}(\mathbf{x},t)$ and which may include regularization. For example, E could be based on the ℓ_2 norm of local instantaneous differences between $T_{ij}(\mathbf{x},t)$ and $T_{ij}^{\mathcal{F}}(\mathbf{x},t)$ over P distinct stencil center points sampled from a region in which the turbulence state – and thus the relation $\mathcal{F}_{ij}$ – is taken to be uniform. This is typically a local region centered on $(\mathbf{x},t)$, but could extend in homogeneous directions or along Lagrangian paths. The sample region could in some cases span the full computational domain, but is typically much smaller to allow $\mathcal{F}_{ij}$ to adapt to local, instantaneous changes in the turbulence state, with the sampling being repeated over the full domain. Regularization in Eq. (4) ensures that $\mathcal{F}_{ij}$ stably generalizes to points in the same turbulence state that were not included in the set of P stencil center points. Once the degrees of freedom in $\mathcal{F}_{ij}$ have been determined in this way, the resulting locally optimal form of $\mathcal{F}_{ij}$ is then used in Eq. (2) to obtain the local, instantaneous value of $\tau_{ij}^{\mathcal{F}}$.

The same procedure can be implemented for any other unclosed quantity. In effect, we solve a local nonlinear system identification problem at the test scale to determine the optimal local instantaneous degrees of freedom in the nonparameteric relation $\mathcal{F}$. This can be repeated at every point and every time in the simulation, so that a new locally optimal relation between the unclosed quantity and all resolved variables is determined at each point

and time. This approach is therefore a fully-adaptive, self-optimizing autonomic closure for coarse-grained equations.

The closure is "autonomic" in the sense that the simulation itself determines the optimal local, instantaneous relation between the unclosed quantity and resolved variables. In particular, $\mathcal{F}$ is free at each point and time to adapt as needed to the relative degree of nonlinear, nonlocal, nonequilibrium, and other turbulence effects in the flow. In a sense, this new closure approach can be regarded as a nonparametric generalization of the dynamic approach used with various prescribed closure models, such as the dynamic Smagorinsky model [3, 4]. Computational costs associated with this autonomic closure can be controlled by limiting the degrees of freedom in $\mathcal{F}$ and reducing the size of the spatio-temporal stencil $(\mathbf{x}', t')$ associated with its inputs.

It will be shown here through *a priori* tests involving τ_{ij} that even simple implementations of this autonomic approach can provide far more accurate closures for unclosed terms than do dynamic versions of traditional prescribed closure models.

Example of a General Nonparametric Relation $\mathcal{F}$. Although any sufficiently general form could be used, here we show an example of a fully general nonparametric relation that may be used for autonomic closure of τ_{ij}. In this example, we choose $\mathcal{F}_{ij}$ in Eqs. (2) and (3) to be a Volterra series [9], namely a sum of multidimensional convolutions over all possible linear and nonlinear combinations of all resolved variables at all points and times. For instance, the Nth-order Volterra series for an M-dimensional multivariate input vector $\boldsymbol{v}(t)$ and scalar output $y(t)$, namely $y(t) = \mathcal{F}[\boldsymbol{v}(t)]$, is given by

$$y\left(t\right) = h^{(0)} + \sum_{n=1}^{N} \left[\sum_{m_1=1}^{M} \cdots \sum_{m_n=1}^{M} \right] \int_{\mathbb{R}^n} h^{(n)}_{m_1 \cdots m_n} \left(\tau_1, \cdots, \tau_n\right) \prod_{p=1}^{n} v_{m_p}\left(t - \tau_p\right) \mathrm{d}\tau_p \,, \tag{5}$$

where $h^{(n)}_{m_1 \cdots m_n}$ are Volterra coefficients that are formally related to partial derivatives of $\mathcal{F}$. For systems with fading memory and bounded inputs, the Stone-Weierstrass theorem guarantees that any continuous function can be represented to within arbitrary precision by a Volterra series of sufficient but finite order [10].

The continuous Volterra series in Eq. (2) can be written in discrete form for implementation in turbulence simulations. For N_v resolved variables on a discrete spatio-temporal stencil with $[N_x, N_y, N_z]$ spatial points and N_t times, the number of variables in the input

vector is $M = N_v N_x N_y N_z N_t$. The resulting Nth-order discrete Volterra series for $\mathcal{F}_{ij}$ is then

$$\mathcal{F}_{ij} = h_{ij}^{(0)} + \sum_{n=1}^{N} \left[\sum_{m_1=1}^{M} \cdots \sum_{m_n=m_{n-1}}^{M} \right] h_{ij,m_1 \cdots m_n}^{(n)} \prod_{p=1}^{n} \widetilde{v}_{m_p} \,, \tag{6}$$

where the lower bounds on the summations span only unique variable combinations while still allowing for variable repetition in the products. In this example, the input vector $\widetilde{\boldsymbol{v}}$ in Eq. (6) consists of $\widetilde{\mathbf{u}}$ and $\widetilde{p}$ at all points and times $(\mathbf{x}', t')$ in the spatio-temporal stencil, namely

$$\begin{aligned} \widetilde{\boldsymbol{v}}(\mathbf{x}, t) = \{ \, & \mathrm{vec}\left[\widetilde{u}_1(\mathbf{x}+\mathbf{x}', t-t') \,\forall\, \mathbf{x}', t' \geq 0\right], \mathrm{vec}\left[\widetilde{u}_2(\mathbf{x}+\mathbf{x}', t-t') \,\forall\, \mathbf{x}', t' \geq 0\right], \\ & \mathrm{vec}\left[\widetilde{u}_3(\mathbf{x}+\mathbf{x}', t-t') \,\forall\, \mathbf{x}', t' \geq 0\right], \mathrm{vec}\left[\widetilde{p}(\mathbf{x}+\mathbf{x}', t-t') \,\forall\, \mathbf{x}', t' \geq 0\right] \, \}^{\mathsf{T}} \,. \end{aligned} \tag{7}$$

Each (ij) in Eq. (6) has a set of coefficients $\mathbf{h}_{ij} \equiv h_{m_1 \cdots m_n}^{(n)}$ which, once determined, allows the stress $\tau_{ij}^{\mathcal{F}}$ in Eq. (2) to be obtained from resolved variables $\widetilde{\boldsymbol{v}}$ on the stencil.

Since Eq. (6) is a sum of all possible multi-point products of all orders among all resolved variables at all locations and times on the stencil, this general relation can represent many mathematical operations among the resolved variables, including multi-point differences and products, spatial and temporal derivatives, filters, and others depending on the coefficients $\mathbf{h}_{ij}$. Thus, in addition to many other fluid dynamically recognizable quantities, the autonomic closure allows τ_{ij} to locally depend on the resolved strain rate but, as previously recommended [11], does not require or impose any such dependence.

For each (ij) in Eq. (6) the total number of coefficients in $\mathbf{h}_{ij}$ is $N_c = (M+N)!/(N!M!)$, so N_c becomes very large as the series order N and stencil size M become large. However, truncation of the series and limitation of the stencil size allows determination of $\mathbf{h}_{ij}$ in the autonomic closure to become sufficiently manageable for implementation in practical turbulence simulations.

Implementation of Autonomic Closure. For example, the objective function in Eq. (4) may be represented using a mean squared error for E with Tikhonov regularization. With $T_{ij}^{\mathcal{F}}(\mathbf{x}, t)$ given by $\mathcal{F}_{ij}$ in Eq. (6), this is equivalent to a damped least squares minimization, namely

$$\min \quad \mathcal{J}_{ij}(\mathbf{x}, t) = \|\mathbf{T}_{ij} - \mathbf{V}\mathbf{h}_{ij}\|^2 + \lambda \|\mathbf{h}_{ij}\|^2 \,, \tag{8}$$

where $\|\cdot\|$ is the ℓ_2 norm, $\mathbf{T}_{ij}$ is a $P \times 1$ column vector composed of the known test stresses $T_{ij}(\mathbf{x}, t)$ at the P stencil center points $(\mathbf{x}, t)$, $\mathbf{h}_{ij}$ is the $N_c \times 1$ column vector of unknown

coefficients, and $\mathbf{V}$ represents the $P \times N_c$ array of all linear and nonlinear combinations of the input vector $\widehat{\widetilde{\boldsymbol{v}}}(\mathbf{x}, t)$, each row of which corresponds to a different stencil center point $(\mathbf{x}, t)$. Here $\widehat{\widetilde{\boldsymbol{v}}}$ is composed of $\widehat{\widetilde{u}}_i$ and $\widehat{\widetilde{p}}$ and is the test-scale analog of $\widetilde{\boldsymbol{v}}$ in Eq. (7). Since $\mathbf{T}_{ij}$ and $\mathbf{V}$ are known at the test scale, Eq. (8) can be solved for $\mathbf{h}_{ij}$. For $\lambda > 0$, the least squares problem is full rank and can be solved as

$$\mathbf{h}_{ij} = \left(\mathbf{V}^{\mathsf{T}}\mathbf{V} + \lambda \mathbf{I}\right)^{-1} \mathbf{V}^{\mathsf{T}}\mathbf{T}_{ij} \,. \tag{9}$$

This smoothly damps small singular values of $\mathbf{V}^{\mathsf{T}}\mathbf{V}$ that would otherwise generate instabilities, and also ensures that the solution is full rank even in the event that $P < N_c$.

Once the local coefficients $\mathbf{h}_{ij}$ are determined at the test scale from Eq. (8), they are projected to the original coarse-grain scale where $\mathcal{F}$ can be used to evaluate the local unclosed quantity, as in Eq. (2). In effect, the local, instantaneous coefficients $\mathbf{h}_{ij}$ characterize the local, instantaneous state of the turbulence, including the extent of nonlinear, nonlocal, nonequilibrium, and other characteristics of the turbulence at that point and time. When the coarse-grain and test-filter scales are sufficiently close, the relative effect of these characteristics should locally be the same in the coarse-grain fields as in the test fields, and thus $\mathbf{h}_{ij}$ should also be the same.

Demonstration and Tests of Autonomic Closure. We now show a simple demonstration of autonomic closure and use it in *a priori* tests to assess the accuracy and utility of this new turbulence closure approach. Specifically, we represent τ_{ij} with the Volterra series form in Eq. (6) and use Eq. (7) to write the input vector $\widetilde{\boldsymbol{v}}$ in terms of $\widetilde{u}_i$ and $\widetilde{p}$ ($N_v = 4$), but we truncate the series after second order ($N = 2$) and use only time-local variables ($N_t = 1$) on a $3 \times 3 \times 3$ spatial stencil, giving $M = 108$ and $N_c = 5995$. The large number of coefficients $\mathbf{h}_{ij}$ is due to the many multipoint second-order products that can be formed from $\widetilde{u}_i$ and $\widetilde{p}$ on even this small stencil.

Using spectrally sharp filters applied to data from a 1024^3 pseudo-spectral direct numerical simulation (DNS) of homogeneous isotropic turbulence at $\mathrm{Re}_\lambda = 433$ in the Johns Hopkins Turbulence Database [12], the velocity and pressure fields are coarse-grained and test-filtered to, respectively, retain 30 and 15 Fourier modes. The sample region here spans the entire domain, although smaller regions could be used instead to reveal local variations in the turbulence state via $\mathbf{h}_{ij}$. Across the sample region we sample at 25 equally-spaced increments along each direction, giving $P = 15,625$ total points and providing an over-

determined system for $\mathbf{h}_{ij}$, which is solved using Eq. (9).

Figure 1 shows typical examples of test stress fields $T_{ij}(\mathbf{x},t)$ and corresponding $T_{ij}^{\mathcal{F}}(\mathbf{x},t)$ fields resulting from the least-squares minimization for $\mathbf{h}_{ij}$. It is apparent that even this relatively simple $\mathcal{F}_{ij}$ is sufficient to represent most of the features in the test stresses $T_{ij}(\mathbf{x},t)$. Also shown for comparison is the corresponding representation of the test stresses from the dynamic Smagorinsky (DS) model of Lilly [4] with no additional averaging or clipping, denoted $T_{ij}^{DS}(\mathbf{x},t)$. The DS model is chosen for comparison due to its widespread use and because, similar to the current approach, it effectively requires the solution of an optimization problem to determine a variable model coefficient. It is apparent from Fig. 1 that the highly prescriptive relation in the DS model between the test stresses and the test-filtered variables is far less able to represent features in $T_{ij}(\mathbf{x},t)$ than the autonomic closure.

Figure 2 shows corresponding results for the turbulent stress field $\tau_{ij}(\mathbf{x},t)$ to allow comparison with the autonomic closure representation $\tau_{ij}^{\mathcal{F}}(\mathbf{x},t)$, which uses the same $\mathbf{h}_{ij}$ determined at the test filter scale in Fig. 1. Also shown for comparison are corresponding results $\tau_{ij}^{DS}(\mathbf{x},t)$ from the DS model. It is apparent that $\tau_{ij}^{\mathcal{F}}(\mathbf{x},t)$ from the autonomic closure provides a remarkably accurate representation of the true stress $\tau_{ij}(\mathbf{x},t)$, especially in view of the global optimization used here, while $\tau_{ij}^{DS}(\mathbf{x},t)$ has nearly no correlation with features in $\tau_{ij}(\mathbf{x},t)$.

Figure 3 uses probability densities to compare test stress values T_{ij} with $T_{ij}^{\mathcal{F}}$ and T_{ij}^{DS}, and turbulent stress values τ_{ij} with $\tau_{ij}^{\mathcal{F}}$ and τ_{ij}^{DS}. The distributions $T_{ij}^{\mathcal{F}}$ and $\tau_{ij}^{\mathcal{F}}$ from the autonomic closure agree remarkably well with the true stress distributions T_{ij} and τ_{ij}, while those from the DS model greatly overpredict the occurrence of large positive and negative stress values.

Figure 4 similarly compares the kinetic energy flux between resolved and unresolved scales, $\widetilde{P}(\mathbf{x},t) = \tau_{ij}\widetilde{S}_{ij}$, with corresponding results $\widetilde{P}^{\mathcal{F}}(\mathbf{x},t)$ from the autonomic closure and $\widetilde{P}^{DS}(\mathbf{x},t)$ from the DS model, each obtained from their corresponding stress fields. It is apparent that the autonomic closure provides remarkably accurate results for $\widetilde{P}(\mathbf{x},t)$ and its distribution, while the DS model essentially matches only the average energy flux and has nearly no correlation with the actual energy transfer field. This is verified in the probability densities in Fig. 5, where even this simple autonomic closure is seen to provide accurate results for the distribution of energy flux values, while the prescribed (DS) closure greatly overpredicts large positive and negative energy flux values.

Summary and Conclusions. The autonomic approach to turbulence closure presented here provides a fully-adaptive, self-optimizing way to treat unclosed terms in coarse-grained equations, based on a locally optimal relation between the unclosed quantity and all resolved variables at each point and time. The nonparametric nature of the approach allows the closure relation to freely adapt to varying nonlinear, nonlocal, nonequilibrium, and other turbulence characteristics throughout the flow. By limiting the degrees of freedom in the general relation and reducing the size of the stencil on which it is implemented, the computational cost associated with the autonomic closure can be managed. Even the simple implementation of the autonomic closure demonstrated here gives remarkably more accurate results than dynamic versions of traditional prescribed turbulence models.

The autonomic approach also provides a means for "model discovery" by finding optimal coefficients $\mathbf{h}_{ij}$ at a test scale that give effective representations for unclosed terms. These coefficients and the associated stencil then provide an autonomically-discovered static model that can be broadly implemented. Furthermore, the resulting $\mathbf{h}_{ij}$ can be decomposed into any desired set of fluid dynamically recognizable quantities that can be formed from the resolved variables on the chosen stencil, thereby providing autonomically-enabled insights into local turbulence physics; e.g., in near-wall turbulence.

This new closure is broadly related to recent applications of machine-learning approaches to turbulence simulations (e.g., [13–16]). A key distinction is that the autonomic closure does not require external training data. In effect, the test fields here provide internal training data and the scale-invariance of local turbulence characteristics between the test-filter and coarse-grain scales allows the local degrees of freedom in the general nonparametric relation $\mathcal{F}$ to be projected from one scale to the other.

We have shown results from *a priori* tests of autonomic closure for LES, but full assessment of the performance and accuracy of this new approach also requires *a posteriori* tests to investigate matters such as numerical stability, computational cost, and closure accuracy for non-spectrally sharp filters. In particular, accurate predictions of forward and backward scatter of kinetic energy, as well as the duration of backward scatter events, are critical for ensuring that the closure is both realistic and stable in simulations. The present results show that both forward and backward scatter of kinetic energy in $\widetilde{P}(\mathbf{x}, t)$ flux fields from the autonomic closure agree well with corresponding DNS fields, in contrast to the largely unphysical fluxes predicted by the dynamic Smagorinsky model. Although some prior models

showing improved agreement in *a priori* tests, such as the similarity model [17], are known to be insufficiently dissipative, it is anticipated that the large number of degrees of freedom in the autonomic closure may enable accurate predictions of backscatter and dissipation across a wide range of local turbulence states. Ongoing work is also exploring whether test filtering can be similarly applied to ensemble-averaged fields in order to allow the approach presented here to extend to autonomic closure of ensemble (Reynolds) averaged turbulence simulations.

---

[1] J. S. Smagorinsky. General circulation experiments with the primitive equations I. The basic experiment. *Mon. Weath. Rev.*, 91:99–164, 1963.

[2] J. W. Deardorff. A numerical study of three-dimensional turbulent channel flow at large reynolds numbers. *J. Fluid Mech.*, 41(02):453–480, 1970.

[3] M. Germano, U. Piomelli, P. Moin, and W. H. Cabot. A dynamic subgrid-scale eddy viscosity model. *Phys. Fluids A*, 3(7):1760, 1991.

[4] D. K. Lilly. A proposed modification of the Germano subgrid-scale closure method. *Phys. Fluids A*, 4(3):633, 1992.

[5] C. Meneveau and J. Katz Scale-Invariance and Turbulence Models for Large-Eddy Simulation. *Annu. Rev. Fluid Mech.*, 32:1-32, 2000.

[6] G. C. Burton and W. J. A. Dahm. Multifractal subgrid-scale modeling for large-eddy simulation. I. Model development and a priori testing. *Phys. Fluids*, 17(7):075111, 2005.

[7] P. E. Hamlington and W. J. A. Dahm. Reynolds stress closure for nonequilibrium effects in turbulent flows. *Phys. Fluids*, 20(11):115101, 2008.

[8] P. E. Hamlington and W. J. A. Dahm. Nonlocal form of the rapid pressure-strain correlation in turbulent flows. *Phys. Rev. E*, 80:046311, 2009.

[9] M. Schetzen. *The Volterra and Wiener theories of nonlinear systems.* Krieger Pub, Malabar, Fla, 2006.

[10] S. Boyd and L. Chua. Fading memory and the problem of approximating nonlinear operators with Volterra series. *IEEE Trans. Circ. Sys.*, 32(11):1150–1161, November 1985.

[11] T. S. Lund and E. A. Novikov. Parameterization of subgrid-scale stress by the velocity gradient tensor. *Center for Turbulence Research Ann. Res. Briefs*, pages 27–43, 1992.

[12] Y. Li, E. Perlman, M. Wan, Y. Yang, C. Meneveau, R. Burns, S. Chen, A. Szalay, and G. Eyink. A public turbulence database cluster and applications to study Lagrangian evolution of velocity increments in turbulence. *J. Turb.*, 9, 2008.

[13] F. Sarghini, G. de Felice, and S. Santini. Neural networks based subgrid scale modeling in large eddy simulations. *Comp. & Fluids*, 32:97–108, 2003.

[14] E.J. Parish and K. Duraisamy A paradigm for data-driven predictive modeling using field inversion and machine learning. *J. Comput. Physics*, 305:758–774, 2016.

[15] J. Ling and J. Templeton. Evaluation of machine learning algorithms for prediction of regions of high Reynolds averaged Navier Stokes uncertainty. *Phys. Fluids*, 27, 085103, 2015.

[16] R. Vishnampet, D. J. Bodony, and J. B. Freund. A practical and efficient discrete-adjoint method for high-fidelity compressible turbulence simulations. *J. Comp. Phys.*, 285:173–192, 2015.

[17] J. Bardina, J. H. Ferziger, and W. C. Reynolds. Improved subgrid scale models for Large Eddy Simulation. AIAA paper No. 80-1357, 1980.

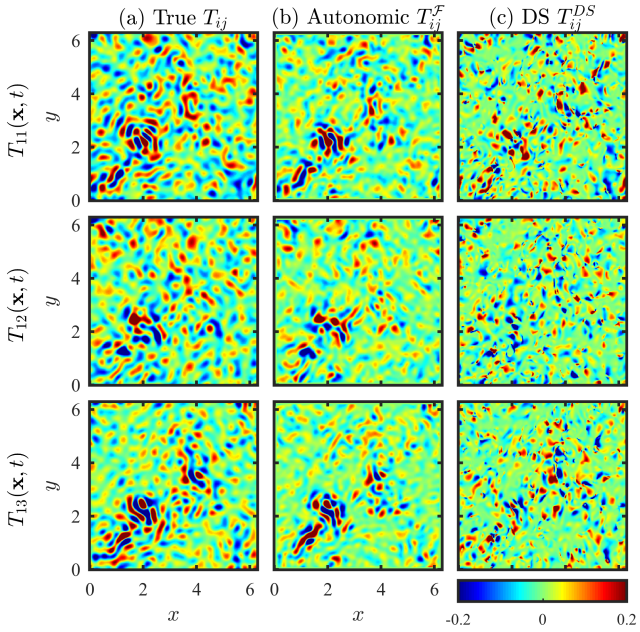

FIG. 1. Test stress fields $T_{11}(\mathbf{x},t)$ (top row), $T_{12}(\mathbf{x},t)$ (middle row), and $T_{13}(\mathbf{x},t)$ (bottom row), showing results for (left column) the true stress $T_{ij}(\mathbf{x},t)$, (middle column) the autonomic stress $T_{ij}^{\mathcal{F}}(\mathbf{x},t)$, and (right column) the stress $T_{ij}^{DS}(\mathbf{x},t)$ from the dynamic Smagorinsky model. (color online)

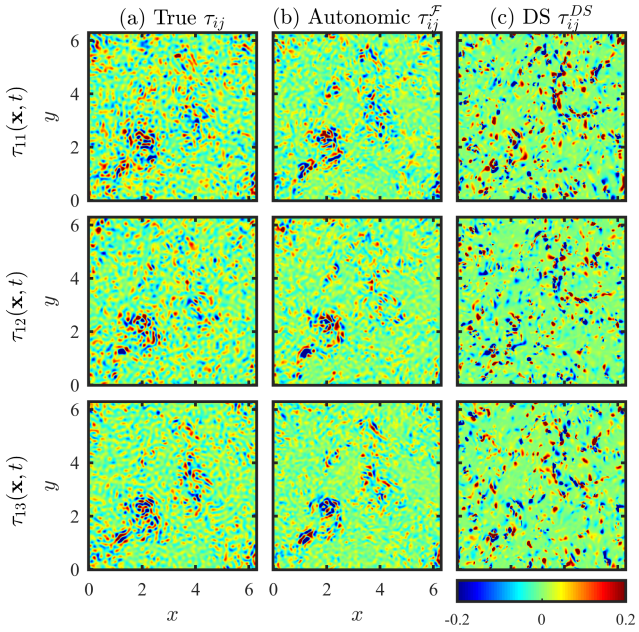

FIG. 2. Coarse-grained turbulent stress fields $\tau_{11}(\mathbf{x},t)$ (top row), $\tau_{12}(\mathbf{x},t)$ (middle row), and $\tau_{13}(\mathbf{x},t)$ (bottom row), showing results for (left column) the true stress $\tau_{ij}(\mathbf{x},t)$, (middle column) the autonomic closure $\tau_{ij}^{\mathcal{F}}(\mathbf{x},t)$, and (right column) the dynamic Smagorinsky model $\tau_{ij}^{DS}(\mathbf{x},t)$. (color online)

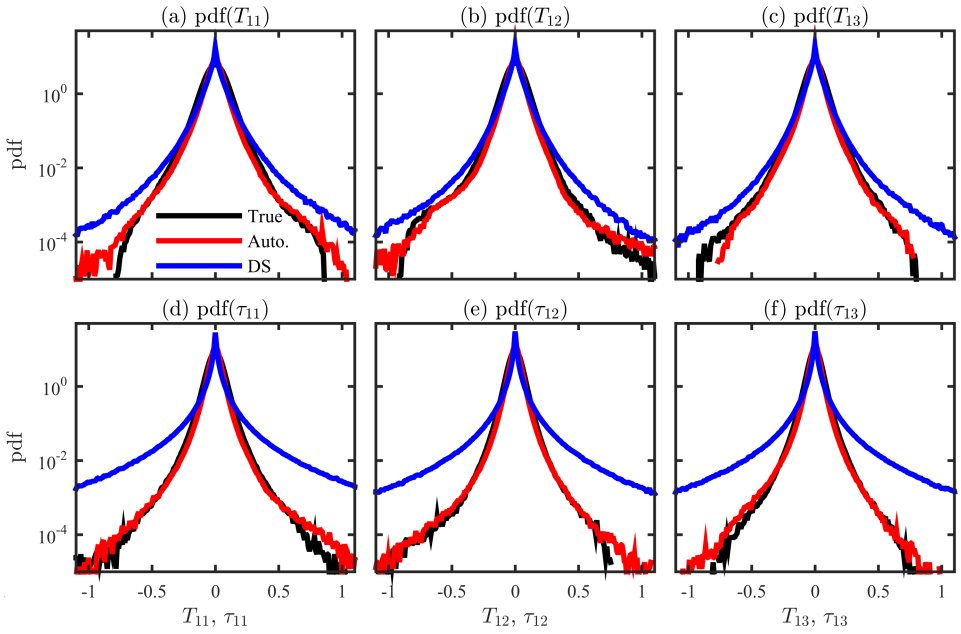

FIG. 3. Probability densities of turbulent stress components at the test-filter scale (top row) and coarse-grain scale (bottom row), showing results for T_{11} and τ_{11} (left column), T_{12} and τ_{12} (middle column), and T_{13} and τ_{13} (right column), showing densities for the true stresses from DNS (black lines), stresses from the autonomic closure (red lines), and stresses from the dynamic Smagorinsky model (blue lines). (color online)

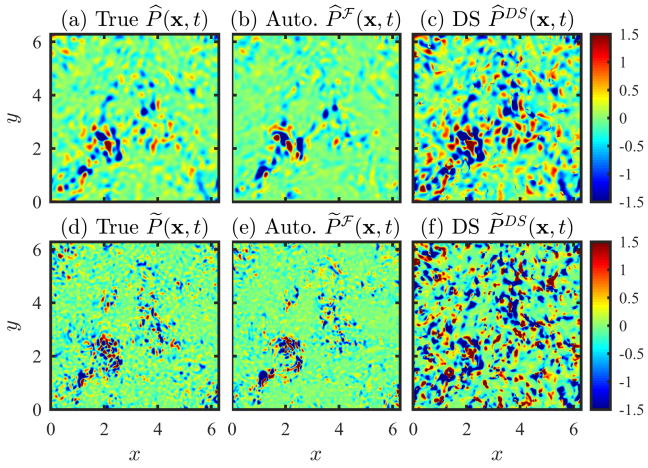

FIG. 4. Kinetic energy flux fields at the test-filter scale (top row) and coarse-grain scale (bottom row), showing results for the true flux fields $\widetilde{P}(\mathbf{x},t)$ (left), the fields $\widetilde{P}^{\mathcal{F}}(\mathbf{x},t)$ resulting from the autonomic closure (center), and the fields $\widetilde{P}^{DS}(\mathbf{x},t)$ from the dynamic Smagorinsky model. Even this simple implementation of autonomic closure is far more accurate than the prescribed closure in the dynamic Smagorinsky model. (color online)

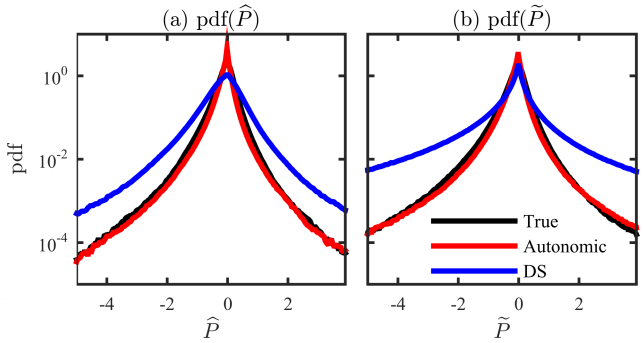

FIG. 5. Probability densities of kinetic energy fluxes (a) $\widehat{P}$ at the test-filter scale and (b) $\widetilde{P}$ at the coarse-grain scale, showing distributions of the true fluxes from DNS (black lines), fluxes from the autonomic closure (red lines), and fluxes from the dynamic Smagorinsky model (blue lines). (color online)